(article starts on next page)

Article

Flame Characterization of Cofiring Gaseous and Solid Fuels in Suspensions

Samuel Colin,* Fredrik Normann, Christian Fredriksson, and Klas Andersson

Read Online

ACCESS | Metrics & More | Article Recommendations

ABSTRACT: This work characterizes technical scale flames of suspension firing of gaseous and solid fuel mixtures through in-flame measurements with focus on nitrogen oxide (NO_x) formation. The aims are to investigate the impacts of substituting a solid fuel with a gaseous fuel on the important mechanisms for NO_x formation and to highlight important considerations for burner design. The investigation was performed in a 100 kW test unit that fires mixtures of propane and lignite. The global emissions levels and in-flame compositions were measured. A detailed reaction model was used to interpret the experimental results. The study highlights the importance of the early release of volatile nitrogen to reduce the levels of NO_x. The findings indicate that substituting lignite by propane is advantageous in terms of reducing NO emissions, primarily due to the diminished input of fuel-bound nitrogen to the flame. However, this holds true only if the flame temperature of the gaseous fuel does not increase excessively. Finally, introducing a relatively small quantity of solid fuel to a propane flame appears to alter the flame behavior to resembles that of the "solid fuel," with a longer and wider flame. Despite this, carbon monoxide and nitrogen oxide concentrations remain like gas combustion but more dispersed.
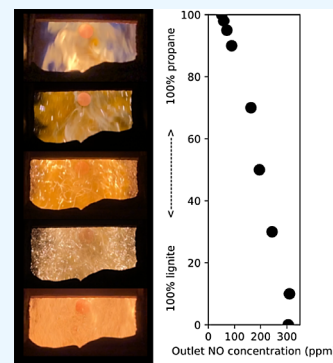
INTRODUCTION

Uncertain energy markets[1] combined with the transition to fossil-free fuels push industry for flexibility in fuel use. The need for reduction in carbon dioxide emission pushes some fossil coal users toward gaseous fuels, like natural gas (limited action to reduce CO_2) or hydrogen, while high gas prices push some industries toward the use of solid fuels.[2,3] Low CO_2-iron making is likely to be at higher cost.[4] Rotary kilns are a commonly used industrial method for high-temperature heating of solid materials, where it is important to retain the flame properties for heating and environmental reasons. A rotary kiln is a continuous processing unit that can be applied to heat various materials, such as lime, cement (1400−1500 °C), and iron ore pellets (1200−1300 °C).[5−7] Given the importance of conserving the flame properties in the kiln, for both the stability of the process and the quality of the final products, new fuels or fuel mixtures should preferably mimic the flame characteristics of the traditional pulverized coal flame. To large deviations in flame characteristics may require redesigns of the process (and potentially the product), which comes at considerable costs. Cofiring may increase fuel flexibility and facilitate the transition toward low-CO_2 processes within existing process designs. High-temperature heating in rotary kilns includes heating of large amounts of secondary air (typical flue gas O_2 concentrations are 1−4% in the cement kiln and 15−17% in the iron ore kiln)[8] and results in significant emissions of nitrogen oxide species (NO_x). The oxides of nitrogen (NOx) have deleterious impacts on the environment and living organisms, including humans.[9] In rotary kiln conditions, air and fuel

stagings through introduction of multiple inlets are challenging, and the focus of this study is on the flame characteristic of fuel mixture of gas and solid fuels with air-to-fuel ratios >1.

NO formation arises through various pathways, with the significance of prompt, N_2O, and NNH pathways deemed negligible or of minimal importance in the studied conditions,[10−18] only thermal NO and fuel NO are investigated.

On the one hand, gaseous fuels may increase NO_x formation through the thermal route as the higher rates of reaction of gaseous fuels, relative to solid fuels, and increase the flame temperature and, consequently, thermal NO_x formation. On the other hand, in pulverized coal combustion, the fuel-bound nitrogen (usually in the range of 0.2−2.5 wt %[19]) has been shown as the major source of NO_x emissions.[14,20−24]

The formation of NO_x in solid fuel combustion units has been thoroughly investigated. The release of nitrogen from coal particles depends on the coal rank and the local combustion conditions (e.g., turbulence, ignition, interaction between homogeneous and heterogeneous forms of combustion, and particle heating rate). In the initial stage of coal combustion, the particles are heated and dried. Heating leads to the

devolatilization of the coal particles and the release of volatile matter followed by the combustion of char. For the volatiles, it is generally accepted that higher-ranked coal release lower levels of volatiles.[25,26] Additionally, higher pyrolysis temperature promotes the release of nitrogen volatiles,[27−31] and higher heating rate also tends to enhance yield of volatiles. The literature proposes that the increased production of volatiles under high heating rates can be explained by two factors: first, the heightened thermal fragmentation of the coal molecular structure, thus inhibiting secondary reactions;[25] second, the migration of fixed carbon into the gas phase.[32] Regarding the generation of NO under rotary kiln conditions, a significant excess of air enhances NOx formation from fuel-bound nitrogen during both volatile combustion and char combustion. An increase in the partial pressure of oxygen amplifies the presence of the key chain carrying radicals O and OH, essential for oxidating volatile nitrogen into NO. Oxygen also promotes conversion of char-bound nitrogen to NO.[33,34] Furthermore, a surplus of oxygen diminishes the availability of char for NO reduction by accelerating char oxidation and dispersing NO and char, thereby decelerating the reaction rate.[35,36]

To predict the release of NO_x, the partitioning of Fuel-N into volatiles and char is important. However, depending on the prevailing conditions, the partitioning of Fuel-N may end up somewhere between 0% and 100% volatiles.[27−31] Song et al.[37] have shown that under conditions of low concentrations of pulverized coal (high level of transport air in the pulverized coal flow), the production of NO_x is dependent upon the levels of both char nitrogen and volatiles nitrogen, whereas under conditions of high concentrations of pulverized coal, NO_x are produced mainly from volatiles nitrogen. NO_x from volatiles are produced mainly at the point of ignition.[44] Nitrogen elements within coal are manifested in various forms, mainly as pyridinic nitrogen, quaternary nitrogen, and pyrrolic nitrogen, producing the dominant intermediary volatile gaseous species NH_3 and HCN, accounting for 90%−95% of the total.[38,39] The remaining nitrogen is present in the form of molecular nitrogen, along with traces of other species, such as CH_3CH, CH_2CHCN, and C_6H_6CN.[39]

The release of HCN and NH_3 is complex but thoroughly investigated.[19,24,40−45] Numerous discussions have arisen regarding the mechanisms underlying NH_3 formation. A review encompasses several hypotheses regarding NH_3 generation during pyrolysis. These hypotheses include NH_3 formation from the quaternary nitrogen (N-Q) functionality in coal,[27] via HNCO as an intermediate,[46] through the hydrogenation of HCN in the gas phase[40] or on the char surface,[47] via the hydrolysis of HCN,[48] and through the direct hydrogenation of coal-N by H radicals.[49] Although discussions are still active about the source of NH_3, regardless, the generation of NH_3 from coal-N, primarily existing in the form of heteroaromatic structures within coal, necessitates a supply of active hydrogen.

Following NH_3 formation, the predominant pathway to NO involves three successive dehydrogenation steps leading from NH_3 to NH_2, then to NH, ultimately culminating in the formation of N radicals.[24] The fate of these radicals is contingent upon local conditions, wherein they may yield either NO or N_2. An active collision between N and NO facilitates the formation of N_2, whereas a collision with O_2, OH, or O radicals leads to NO formation. As demonstrated by Miller et al.,[24] indirect pathways from NH_2 and NH to NO are also viable. NH_2, when exposed to O radicals, can potentially transform into HNO, which in turn may evolve into NO in the presence of primarily OH and NH_2. Similarly, NH can give rise to NO in the presence of O and may indirectly generate NO via intermediate HNO.

Regarding the pathway from HCN to NO, it is agreed that the thermal degradation of released volatiles and char during pyrolysis represents a primary pathway for the formation of HCN. A principal proposed pathway for the conversion of HCN to NO, as elucidated by Thorne et al.,[50] involves intermediary species NCO and NH. In this mechanism, HCN may react with O radicals to produce NCO, which can subsequently react with H radicals to form NH. The transformation of NH to NO follows a similar path as described earlier for NH_3. Alternatively, Miller et al.[51] propose an alternate route through the intermediary species CN. In this pathway, HCN can react with H, O, or OH radicals to yield CN, which can then further react to form NCO in the presence of OH and O_2, or transform into N radicals in the presence of O.

The distributions of HCN and NH_3 in the volatiles are difficult to predict. As an example, Kambara et al.[39] showed that for various ranks of coal (volatiles contents ranging from 22% to 79.3%), HCN predominate, and a lower NH_3/HCN ratio is observed at higher temperature. Other studies have shown that the amount of HCN increases with higher rank of coal.[20,52] NH_3 dominating the HCN has been reported[53] in coal devolatilization; however, it is in a condition of low rank of coal and devolatilization temperature below 900 °C.

The literature on the cofiring of gaseous and solid fuels is limited.[54−57] Ueki et al.[54] have reported that the introduction of gaseous fuels to a coal flame is likely to increase the coal heating rate, resulting in faster release of volatile matter. Furthermore, the early oxidation of gas may decrease the rate of char devolatilization by reducing the O_2 concentration around the char particles.[54,58] Moreover, gaseous injection may decrease NOx formation, by increasing the heating rate of coal particles, enhancing the distribution of the nitrogen content in fuel into volatiles nitrogen.[59] Other works have been performed with the cofiring of gaseous fuel and solid fuels, including natural gas and coal, with the focus on blast furnace operation,[60,61] and propane and coal combustion under fluidized bed conditions.[58] However, those studies did not focus on the NO_x formation.

The present work investigates the impacts of substituting solid fuels with gaseous fuels in high-temperature flame combustion through measuring the emissions levels and mapping the in-flame conditions in technical-scale experiments. The experimental results are interpreted and discussed with the help of detailed reaction modeling that extends the present understanding of NO_x formation during combustion to identify important design considerations.

■ METHODS

This section presents the experimental unit and the test cases, as well as the model that was developed to analyze the experimental results.

The experiments were conducted in a Chalmers 100 kW combustion unit. The unit consists of a cylindrical refractory furnace with an inner diameter of 80 cm and height of 240 cm. Inside the furnace, there are four water-cooled rods positioned near the wall that extract heat from the combustion process and stabilize the flame. Air and fuel are injected at the top of the furnace using a multifuel burner, which can be operated with both gaseous and solid fuels. The furnace and the burner are presented Figure 1. The fuels used were propane and lignite. The properties of lignite are listed in Table 1. The burner is designed with central solid fuel feeding and annular fuel gas injection
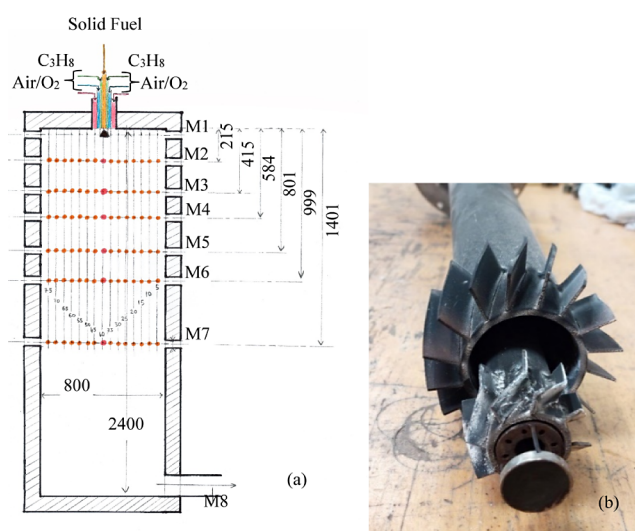
Figure 1. (a) Schematic of the Chalmers 100 kW unit showing all the ports used for in-flame measurements. (b) The head of the burner, showing the outer swirl, inner swirl, outer propane holes, centered solid fuel flow, and a cone below the fuel flows.

Table 1. Properties of the Lignite Used in the Experiments

		lignite
Cal	MJ/kg dry	23.8
LHV	MJ/kg dry	22.9
moisture	%wt	10.2
ash	%wt dry	5.6
volatile	%wt dry	57.9
C-fix	%wt dry	36.5
C	%wt dry	61.8
H	%wt dry	4.4
O	%wt dry	26.9
N	%wt dry	0.7
S	%wt dry	0.659
Cl	%wt dry	0.017

through a perforated plate with eight holes. These gas injection holes are further surrounded by two swirled air feeders, with a −45° angle for the inner air and 15° angle for the outer air. At the outlet of the burner, there is a cone that helps to spread the solid fuel for improved combustion stability. Under cofiring conditions, the cone ensures mixing of the two fuels, i.e., rather than maintaining separate flows of the gaseous and solid fuels.

To allow for optical and physical access to the flame, seven measurement ports (M1−M7) are installed on the side of the furnace. Eight additional ports (M8−M15) are installed along the flue gas channel after the furnace. This experimental setup has been used in several previous campaigns, and further information can be found elsewhere.[62,63]

The measurement techniques included gas and temperature analyses. Gas concentrations were measured in the flame through ports M2 to M5 at horizontal depths of 5, 30, 35, and 40 cm from the inner wall, as well as in the flue gas through port M8. A probe with an outer diameter of 45 mm and an inner diameter of 8 mm was used to extract the gas samples. To protect the probe from the flame, the outer shell of the probe is water-cooled, and to prevent condensation of the gas sample, the inner tube of the probe is heated to 140 °C using an electric heater. Fourier-transform infrared spectroscopy (FTIR) was used to measure the wet gas concentration, while a natural gas analyzer (NGA) was used to measure the oxygen levels. Temperature measurements were conducted with two types of suction pyrometers for the gaseous and solid fuel combustion processes. Both suction pyrometers apply a Type S thermocouple, which is cooled and shielded from flame radiation; only the solid fuel probe was protected from particles by a ceramic shell. The two types of pyrometers showed significant discrepancies in relation to the measured temperatures of the propane flame: the gas probe measured peak temperatures in the range of 1,650°−1,730 °C, while the solid fuel probe gave a temperature of around 1,450 °C at the same location. The gas probe is sensitive to particles and is not suitable for use under solid fuel-firing conditions. The temperature measurements were obtained by positioning the probe at M2 and moving it horizontally within the flame to capture the highest temperature for each case. It should be noted, however, that these recorded data do not represent the absolute maximum temperatures of the flame but rather serve as an indication of the temperature's evolution across different cases.

Two series of experiments were conducted: 1) mapping of the in-flame gas concentrations and 2) screening of fuel mixtures ranging from 100% propane to 100% lignite. The test cases for in-flame mapping included: 100% lignite; 50% lignite and 50% propane; and 100% propane. Test cases for the screening included four screenings. The sequence for the screening tests was as follows (percentage propane): 100%, 98%, 95%, 90%, 70%, 50%, 30%, 10%, and 0%. Measurements were not taken between 10% and 0% propane because the propane flow rate was too low for stable operation.

Table 2. Theoretical Values for Inlets and Outlets of the Examined Cases Were at a Stoichiometric Air-to-Fuel Ratio of 1.15

cases	fuel flows			fuel gas concentrations			
gas/solid fuel	C_3H_8	lignite	total air flow	O_2	CO_2	H_2O	exhaust gas flow
%	[g/s]	[kg/h]	g/s	[% dry]	[% dry]	[%]	g/s
100	1.73	0.00	31.01	2.95	11.82	13.61	32.74
98	1.69	0.24	30.91	2.95	11.92	13.53	32.66
95	1.64	0.61	30.75	2.95	12.08	13.41	32.55
90	1.56	1.21	30.49	2.94	12.33	13.20	32.36
70	1.21	3.63	29.45	2.90	13.40	12.34	31.60
50	0.86	6.05	28.40	2.86	14.51	11.41	30.84
30	0.52	8.47	27.36	2.83	15.68	10.42	30.09
10	0.17	10.89	26.32	2.78	16.90	9.36	29.33
0	0	12.10	25.80	2.77	17.22	8.79	28.95

Table 3. Summary of the Model Gas and Solid Fuel

combustion characteristic(s)	model
kinetics	The detailed reaction mechanism used is described by Mendiara and Glarborg[64] involving 97 species and 779 elementary reactions.
mixing	Mixing is delineated by the rate at which air is introduced to the fuel along the axial direction. Mixing profiles align with the lowest oxygen measurements in the flame: central line for propane and 10 cm off the central line for lignite. Microscale mixing phenomena, such as eddies and vortices, are not taken into consideration.
heat release, heat transfer, and temperature	The energy equation is not solved. Instead, for both models, the temperature profile is given by the measurement of the maximum temperature of the respective flame in each port from M2 to M5. The peak temperature is located at 21.5 cm (port M2 in the Chalmers unit).
fuel composition	Propane: C_3H_8 (1.73g/s) Fuel-N: HCN: [0, 0.00142, 0.00284, 0.00567, 0.0113, 0.0227, 0.0454, 0.0908] representing a N-content in fuel (%-mass) of: [0, 0.022, 0.044, 0.088, 0.18, 0.35, 0.7, 1.4]
ignition and pyrolysis	The initiation of ignition is fundamentally governed by kinetics and relies on temperature and gas composition. The reaction rates are expressed in the form of the Arrhenius equation: $k = AT^\beta \exp(-Ea\,RT)$, with Ea is the activation energy [cal/mol], A the pre-exponential factor [cm mol s], and β the temperature exponent. These three parameters are mandatory inputs for the gas-phase kinetics package.
particle characteristics	Properties concerning solid particles, such as porosity, surface area, fragmentation, and swelling, are disregarded.
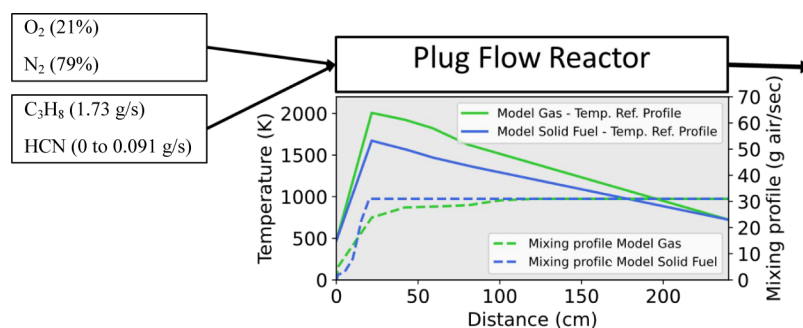
Figure 2. Inputs to the plug flow reactor: C_3H_8 with/without HCN; and O_2 plus N_2. The temperature profiles are on the y-axis on the left. Air flow (O_2 and N_2) is added at the mixing rate given on the y-axis axis on the right. The x-axis indicates the distance from the fuel inlet in the PFR.

- Screenings 1 and 2 were conducted with the same settings. To ensure repeatability, the first screening test was run and then reversed back to 100% propane. The transport air flow rate was set at 130 l/min, and the air-to-fuel ratio was set at 1.15.
- Screening 3 was performed at a transport air flow rate of 70 l/min and air-to-fuel ratio of 1.15.
- Screening 4 was performed at a transport air flow rate of 70 l/min and air-to-fuel ratio of 1.623. This air-to-fuel ratio matches the NO (ppm)/CO$_2$ (%) ratio of 40 ppm/ % for a full-scale coal-fired rotary kiln.

The air flows were adjusted to match the fuel flows and to control the oxygen concentrations in the exhaust gases. Even though the air-to-fuel ratio is kept constant, the distributions of air between burner registers are not equal. Moreover, solid fuel requires transport air, while this is not needed during operation with pure gas. Thus, for the in-flame mapping test with 100% propane, air was introduced via only the two outer air registers of the burner. However, for the screening tests, the transport air flow was kept on during pure propane combustion to maintain the same settings. For all of the screenings, the gas concentrations were measured at M8. For Screenings 3 and 4, the maximum temperature in port M2 was measured by moving the probe horizontally to obtain the highest values. The examined cases are presented in Table 2.

Modeling. A detailed reaction model in CHEMKIN format was used to discuss the impacts of the fuel nitrogen content, combustion temperature, and volatile release on the nitrogen chemistry during solid fuel substitution with gaseous fuels. The specific settings for the models are given in Table 3. The setups of the models are depicted in Figure 2. The model is a plug flow reactor (PFR) with mixing and temperature profiles derived from measurements. A similar modeling approach have successfully been used previously by for example Edland et al.[8,62] It should be noted that the models do not claim to mimic the experiments or uses for CFD, but are barley applied to discuss nitrogen and combustion chemistry under the given conditions, such as temperature profiles, peak temperature location, gas velocity, volatiles profiles, volatiles-N (Vol-N), and mixing profiles.

Two modeling configurations were established: Model Gas was based on the propane-firing conditions, and Model Solid Fuel was based on the lignite combustion conditions. Both models were executed with various fuel mixture configurations, including a baseline of C_3H_8 in mixtures with volatile-N species to represent the fuel bound nitrogen; the mass flow of C_3H_8 is constant between all cases. Devolatilization is not modeled; however, different volatile release rates and distributions between HCN and NH_3 are evaluated—the majority of the results are presented for 100% HCN to simplify discussions. Char behaviors are not included in the modeling. Corelations for prediction of volatile release exist,[24] although highly dependent on fuel and conditions. Therefore, this work applies a sensitivity analysis of the results to the type of volatile release (HCN and/ or NH_3).

To discuss the influence of process parameters on the results, a modeling sensitivity analysis is conducted. Note that the below-mentioned parameters are not calculated (like in so-called CFD simulations) but rather given as an input value. The analysis includes:

- Temperature profile (peak temperature ±200 C maintaining the inlet and outlet temperatures).
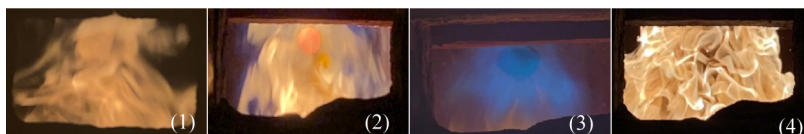
Figure 3. Photographs taken at port M2 with 100% propane firing at flow rate of 1.73 g/s for: (**1**) lambda of 1.15 without transport air; (**2**) lambda of 1.15 with 70 l/min transport air; (**3**) lambda of 1.15 with 1300 l/min transport air; and (**4**) lambda of 1,623 with 70 l/min transport air.

- Heating rate (peak temperature reached at between 5 and 21.5 cm from the fuel inlet).
- Type of volatile nitrogen release HCN/NH$_3$.
- Mixing profiles, and lambda values (1.15 and 1.623).
- Volatile release rate (location and injection rate of Fuel-N).

The *Results* section focuses on results from the reference settings and from settings with significant impact on the results.

After validation, the model was used for several cases in investigations that considered: 1) the relative importance of thermal NO$_x$ formation; 2) the impact of the devolatilization rate; and 3) the difference in flame characteristics between solid and gaseous fuel firings.

To quantify the distribution of NO formation between the fuel-bound nitrogen mechanisms and thermal formation, HCN was introduced to a propane flow with the added amount of nitrogen (in the form of HCN), representing a nitrogen content of the solid fuel that ranged from 0 to 1.4 wt % of the fuel.

To evaluate the impacts of early devolatilization and HCN release, HCN was injected at different rates (for the case representing the lignite with Fuel-N content of 0.7%-mass). Twelve profiles were examined, in which HCN was injected linearly between 0 and 1, 10, 20, 30, 40, 50, 60, 70, 80, 90, 100, and 200 cm, respectively.

To determine whether NO formation during cofiring follows a solid fuel characteristic or gaseous fuel characteristic, both models were run with 100% C$_3$H$_8$ (80 kW) as the reference, with gradual addition of HCN, giving 0%−1.4% Fuel-N (in mass) in the fuel. The total air flow is 31.01 g/s, representing a lambda value of 1.15. The evolutionary profiles of NO for both models were compared with data from screening experiments.

■ RESULTS

The experimental results are presented in the first section and are subsequently discussed and interpreted by using the detailed reaction models.

Flame Visualization. The shape of the flame varied considerably between the scenarios. In Figure 3, a comparison is made between the images of the propane flames captured at M2 in the 80 kW unit. Images 1, 2, and 3 show propane flames with a lambda value of 1.15 without transport air, with 70 l/min of transport air, and with 130 l/min of transport air, respectively. Image 4 shows a propane flame with a lambda value of 1.623 and 70 l/min of transport air. The images in Figure 4 show the flame shape for two screenings with 70 l/min of transport air at two lambda values, along with the three points mapped for the in-flame gas concentration.

Temperature. Regarding the results for temperature and flame characterizations, the highest temperature measured at M2 by the suction pyrometer at a lambda value of 1.15 indicates that the temperature decreases as one progresses from 100% propane to 95% propane, followed by an almost constant temperature level along the screening trajectory from 95% to 50% propane. Subsequently, there is a more-pronounced

decrease in temperature from 1,430 °C at 50% propane to 1,200 °C at 0% propane. The overall decrease in temperature with the addition of solid fuel can be attributed to the slower reaction rate of the solid fuel generating a longer and larger flame.

Increasing the air-to-fuel ratio increased the M2 temperature from 1,200 °C to 1,330 °C for the 100% lignite case. No significant influence of the air-to-fuel ratio on temperature was observed for the cocombustion cases. Nevertheless, a more intense flame was detected with propane at the higher lambda value.

While the temperature increased along with the propane ratio, the rate of increase was higher for 100% lignite to 50% lignite than for 50% lignite to 0% lignite. A higher lambda value showed a similar trend, with a slightly lower increase in temperature following increases in the propane ratio.

In-Flame Gas Concentrations. Three cases were investigated: 100% lignite and a mixture of 50% lignite and 50% propane and 100% propane. Figure 5 displays the results of the in-flame measurements for NO, CO, O$_2$, HCN, and NH$_3$. The standard deviation, minimum, and maximum values are presented in Figure 6. All of the cases were at a power output of 80 kW and a lambda value of 1.15. The lignite cases were operated with a transport air flow of 130l/min, while the propane flame was run without any transport air. A colormap is utilized to represent the measured gas concentrations, with the black points indicating the measurement positions. Linear interpolation is employed at these points. The x-axis represents the diameter of the furnace, while the y-axis represents the distance from the burner inlet. Measurements were taken from M2 to M5, specifically at distances of 215 and 801 mm, respectively, from the burner, on one side of the center line (5−40 cm), and the data were mirrored to create the complete image. No measurements were performed between the burner and the distance of 215 mm and between the wall and 5 cm from the wall.

Flame Characteristics. The pure lignite case exhibits a wider flame with a high concentration of O$_2$ in the center. The addition of propane results in a more-centralized flame with a low concentration of O$_2$ in the center of the flame and high concentrations of O$_2$ at the sides of the flame. In the case with 100% propane, the concentrations of CO and O$_2$ indicate a larger reaction area than those in the other cases. This may be attributed to the momentum of the gas being reduced when operated without transport air.

Comparing the 100% lignite case with the 50% lignite case, it is clear that NO formation occurs closer to the burner when a higher proportion of lignite is used. A significant zone with high NO concentration is observed around 40 cm from the burner, within a distance of 10 cm from the center line. In the case of 50% lignite, the highest NO formation is observed on the sides of the flame, at between 40 and 60 cm, forming a thin line at 10 cm from the center line.

**Volatiles Release in the Condition with Gaseous Fuel Addition.** Figure 5, panels (a) and (b) present the

Figure 4. Photographs taken at M2: (a) lambda 1.15, 70 l/min transport air; (b) lambda 1.623, 70 l/min transport air; (c) lambda 1.15, 130 l/min transport air—only three cases are presented for these settings. The following cases were studied: (**1**) 100% lignite; (**2**) 10% propane, 90% lignite; (**3**) 30% propane, 70% lignite; (**4**) 50% propane, 50% lignite; (**5**) 70% propane, 30% lignite; (**6**) 90% propane, 10% lignite; (**7**) 95% propane, 5% lignite; and (**8**) 100% propane.

concentrations of volatile compounds NH_3 and HCN normalized to the quantity of solid fuel introduced. HCN is the predominant species over NH_3 in terms of the nitrogen volatiles released. The characteristics of HCN and NH_3 release change significantly when propane is added to the lignite flame. With the presence of gas, the volatiles seem to be enhanced. For the lignite flame, the volatiles are seen at the flame sides and spread over a large area, [see Figure 5a]. In the case with 50% propane [Figure 5b], HCN is instead seen at the center line. HCN is observed in oxygen-lean areas of the flame. The NH_3-to-HCN ratio seems to decrease when propane gas is added to the solid fuel flame, which may be attributed to higher flame temperatures. This has been also reported previously.[27,39]

NO Concentration. The NO concentrations measured at M8 during the firing of lignite/propane mixtures are shown in

Figure 7 for the two transport air flow settings (70 and 130 l/min) and the two lambda values (1.15 and 1.623). The concentration presented here is a time average from a period of stable operation. The minimum and maximum concentration measures during the period are also shown. The standard deviation of the measurements varies between 1 and 5 ppm without any correlation, which is considered to be good. The theoretical outlet NO concentrations for Fuel-N conversions of 20%, 30%, and 50% are also provided for reference.

Regarding NO formation, the outlet concentration of NO increased with the proportion of lignite to total fuel. However, the increase was not linearly related to the Fuel-N content in all cases. Three zones are identified, presented with separated trend lines, with high, middle, and low proportions of lignite to total fuel. At high lambda values, a notable increase in NO emissions
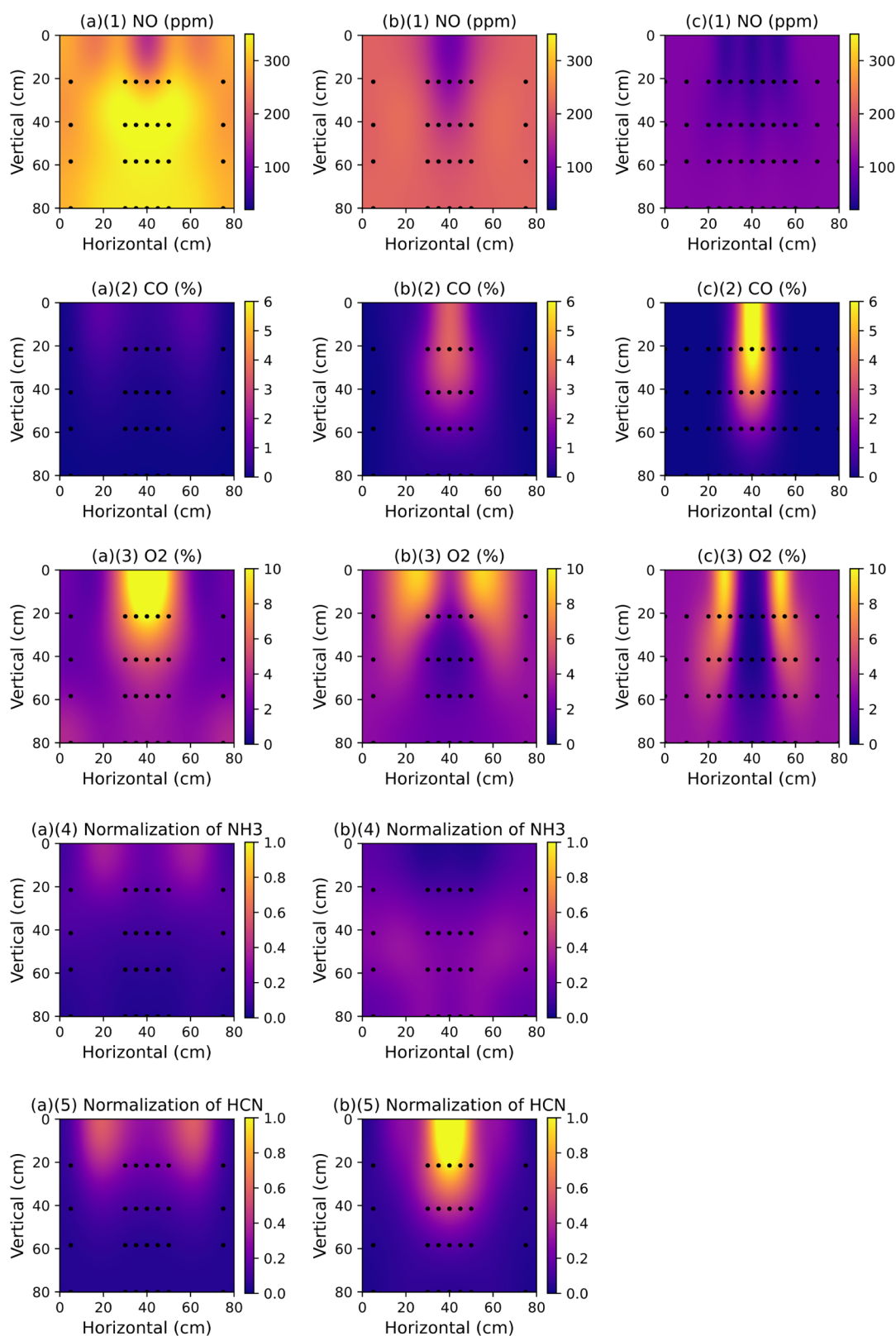
Figure 5. Contour maps of the in-flame gas concentrations for the: (a) lignite flame; (b) 50% lignite, 50% propane; and (c) propane flame. The gas concentrations are for: (**1**) NO; (**2**) CO; (**3**) O_2; (**4**) NH_3; and (**5**) HCN.

is observed from 70% lignite to 100% lignite. Two significant factors may contribute to this phenomenon. First, the temperature, as indicated by the suction pyrometer, exhibited an ascending trend with the increase in lignite. Second, cessation

of gas flow may lead to an augmentation in in-flame O_2 concentration. For the lambda value of 1.15, the formation of NO remained unaffected by the presence of fuel-bound nitrogen when employing high lignite ratios (>90%). While a higher
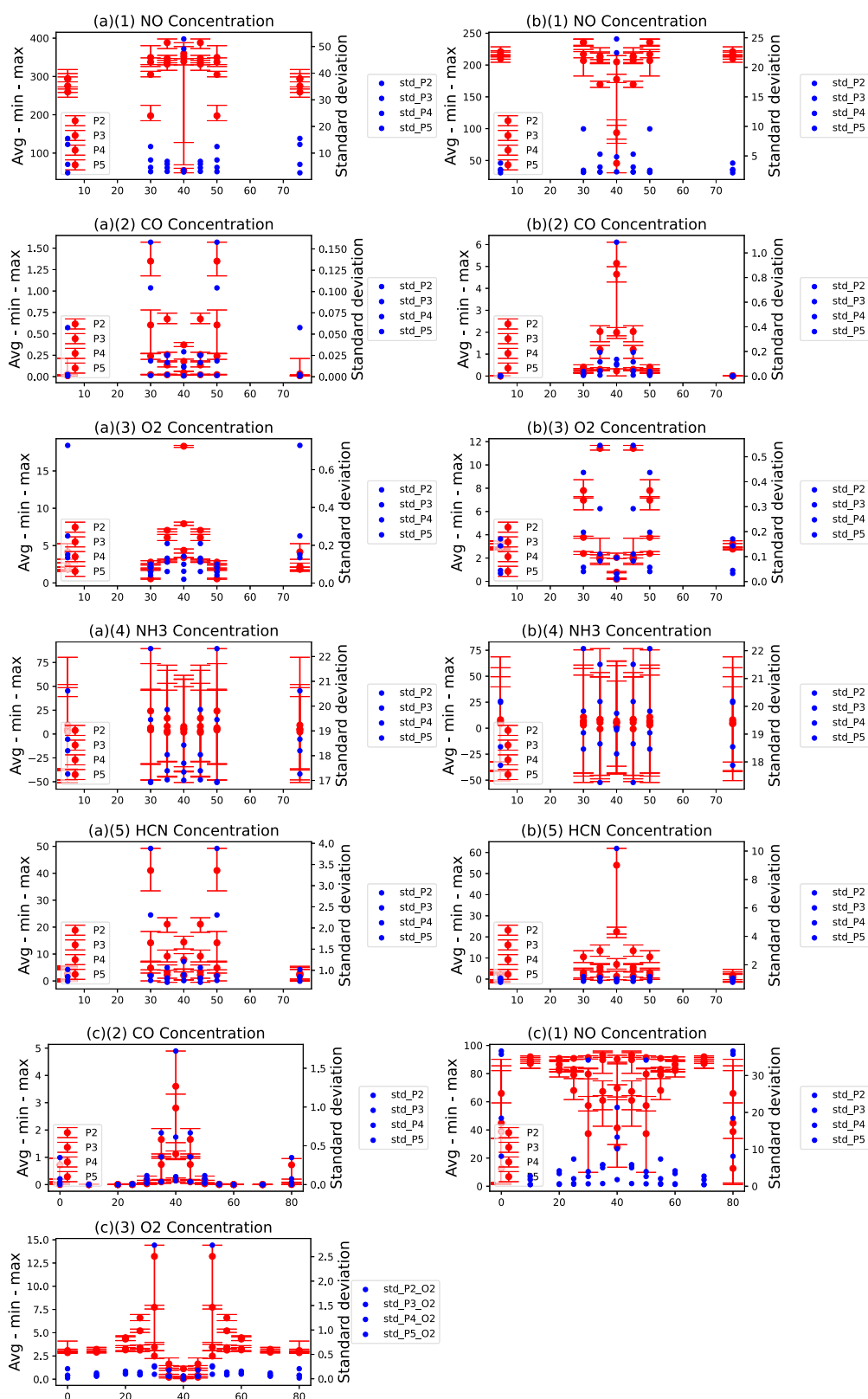
Figure 6. Average, minimum, maximum, and standard deviation of the in-flame gas concentration measurements: NO (**1**), CO (**2**), O_2 (**3**), NH_3 (**4**), HCN (**5**); case of 100% lignite (a), 50% lignite 50% propane (b), and 100% propane (c).

formation of NO (approximately 10% higher in Fuel-N) was anticipated for the 100% lignite composition, consistent measurements yielded nearly constant NO concentrations for both cases. Beyond the augmentation of Fuel-N content in the

100% lignite scenario, several other factors may contribute to the effects of propane inclusion (in the 90% lignite case). First, the propane could potentially accelerate the heating rate of solid fuel particles, facilitating the devolatilization and, subsequently, NO

reduction by Char-N. Second, the propane might broaden the region within the flame where oxygen (O_2) is restricted. Third, the addition of propane could elevate thermal NO levels. Lastly, the incorporation of propane led to enhanced flame stability. An explanation for the absence of reduction in NO emissions between the 100% lignite and the 90% lignite scenarios may be that the introduction of propane is insufficient to markedly deplete the oxygen content within the flame, and the consequent rise in temperature serves as a compensatory mechanism for the decrease in Fuel-N, through an elevation of thermal NO levels.

In the middle range (20%−70% lignite to total fuel), the level of NO formation was found to be proportional to the amount of Fuel-N introduced and was dependent upon the lambda value and transport air flow rate. Decreasing the transport air from 130 to 70 l/min increased the level of NO. The level of NO increased even further when transitioning from lambda 1.15 to lambda 1.623, although all these settings followed the same trend of NO increase with a higher level of lignite.

At a lignite proportion of 20% and below, the level of NO formation was proportional to the amount of Fuel-N introduced at a lambda value of 1.15. However, at the higher oxygen concentrations, for a lambda value of 1.623, there was a significant increase in the level of NO formation, as compared to that at a lambda value of 1.15. In addition, there was a slight increase in the NO concentration between the 90% propane and 100% propane cases, which is assumed to be due to an increase in the level of thermal NO.

Under the lambda 1.623 condition, at >90% lignite, it is expected that the higher level of oxygen, coupled with higher temperatures, promotes thermal NO formation. Furthermore, a delay in the ignition of the flame may contribute to the increase in NO formation. This will be discussed further in the next section.
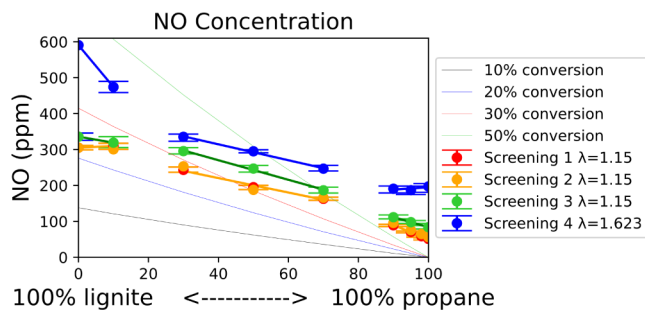

Figure 7. Measured NO concentrations at M8 (outlet) for the fuel range of 100% propane to 100% lignite and theoretical NO concentration given a 10%, 20%, or 30% Fuel-N conversion to NO. Center points are the measured average and error bars gives the maximum and minimum concentration at each point.

Partitioning the Fuel-N Responsibility for a Lambda Value at 1.15. The temperature of the lignite flame was significantly lower than that of the propane flame, although it produced a higher level of NO, indicating that Fuel-N dominated the NO formation over thermal NO formation. With the assumption that the thermal NO formation is constant between the propane and lignite cases, the Fuel-N contribution to the total NO formation is 83% in the pure lignite case. It should, however, be noted that 1) a clear separation of Fuel-N and thermal NO is not possible as there are interactions between the mechanisms and 2) the thermal-NO formation is probably lower in the lignite flame as the temperature is lower, although

also the oxygen availability is lower in the high temperature zones.

Comparison between the Kinetic Model and the Experimental Results. This section compares the data from the in-flame measurements and the modeling results.

Figure 8 shows the measured CO concentrations at the center lines (35 and 40 cm from the wall) for ports M2 to M5, as well as
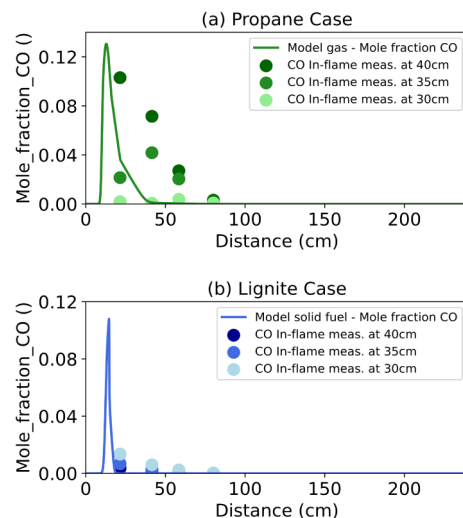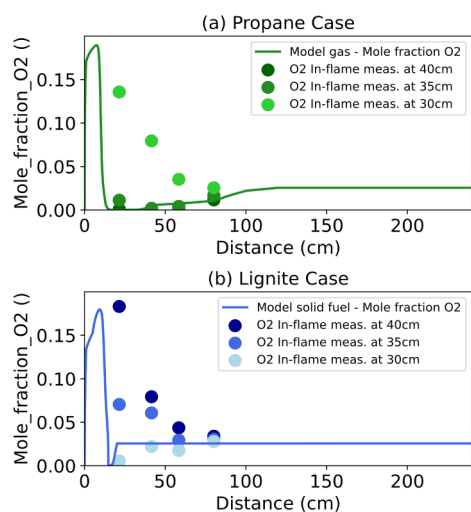

Figure 8. Comparison of the levels of CO for the Model Gas (a) and Model Solid Fuel (b) and the in-flame CO concentrations measured for 100% propane (a) and 100% lignite (b) at horizontal distances at 30, 35, and 40 cm (center line) and vertical distances from M2 to M5.

the calculated CO concentrations for the Model Gas (green) and the Model Solid Fuel (blue). The x-axis represents the distance from the fuel inlet. The Model Gas displays a CO concentration profile representative of the measurements from 40 cm (centerline) to 30 cm from the wall. For the Model Solid Fuel, after 20 cm, the CO level is close to zero, fitting the experimental data for the CO concentration at the center line and at 35 cm.

Figure 9 displays the calculated and measured O_2 concentrations. Model Gas represents the O_2 concentrations measured at the center line, while Model Solid Fuel represents the experimental data measured at 10 cm from the center line (where the lowest oxygen (O_2) concentration was measured). The difference in modeling procedure is due to the flame characteristics of the propane and lignite flames. For lignite, the main reaction zone is shifter outside of the centerline.

Figure 10 compares the calculated and measured NO concentrations, showing that the evolutionary profile of the in-flame NO concentrations accords well with the calculated data.

Comparing Models with Introduction of HCN or NH_3. The sensitivity to the type of volatile nitrogen species released is presented in Figure 11. Each data point represents the NO concentration in the outlet for each model run, for each quantity of Fuel-N per species. In total, the Solid Fuel model underwent 20 runs, while the Gas model underwent 14 runs. For high temperatures (Model Gas), NH_3 versus HCN species do not affect the results. However, at lower temperatures (Model Solid Fuel), a substantial increase in outlet NO concentration is observed when the Fuel-N is represented by NH_3 instead of HCN. As the NH-bound is weaker than the NC-bound,[13] NH_3 may release N-radicals faster at lower temperature,[45] increasing the presence of N-radicals in the high temperature area of the

Figure 9. Comparison of O_2 levels for the Model Gas (a) and Model Solid Fuel (b) and the in-flame O_2 concentrations measured for 100% propane (a) and 100% lignite (b) at horizontal distances of 30, 35, and 40 cm (center line) and vertical distances from M2 to M5.
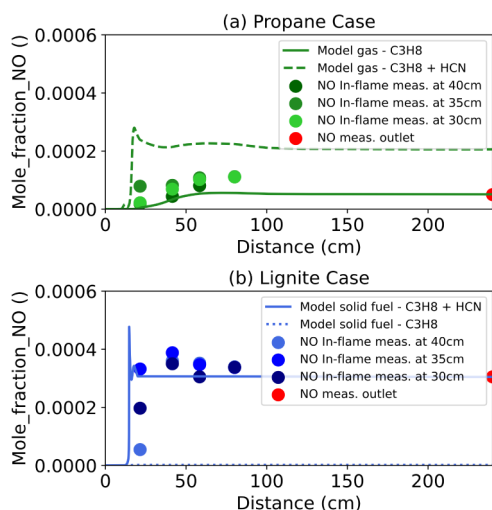
Figure 10. Comparison of the NO levels for the Model Gas with and without HCN (a) and the Model Solid Fuel with and without HCN (b) and the in-flame NO measurements for 100% propane (a) and 100% lignite (b) at horizontal distances of 30, 35, and 40 cm (center line) and vertical distances from M2 to M5.
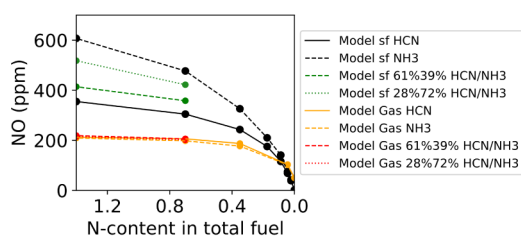

Figure 11. Comparison of outlet NO concentration using HCN, HCN/NH3 mixture, or 100% NH3 as representation of Fuel-N for both the Model Gas and the Model Solid Fuel (sf). Two intermediate mixtures are presented: a mixture of 61% HCN and 39% NH3 representing 50% of Fuel-N in HCN, and another mixture of 28% HCN and 72% NH3 representing 80% Fuel-N in HCN.

Model Solid Fuel. At higher temperatures, however, the temperature is sufficient to also break the NC-bound at the

early stage of combustion. During modeling, the HCN/NH_3 is introduced at the inlet and N-radicals from Fuel-N are quickly oxidized, hindering downstream reduction of NO by N-radicals. However, in the case of continuous injection of HCN, a downstream reduction of NO by N-radicals is observed.

NO Formation During Cofiring—Solid Fuel and Gas Models. Figure 12 shows the relationship between the outlet NO concentration (*y*-axis) and the N-content of the fuel (*x*-axis). The experimental data shown are for a lambda value of 1.15.
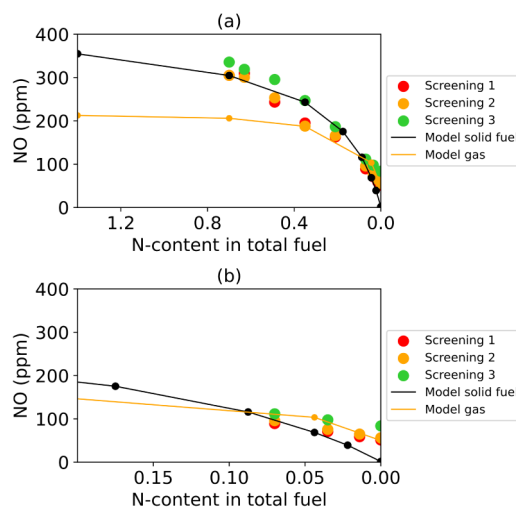
Figure 12. Calculated outlet NO concentrations, which are dependent upon the N-content of the total fuel, were obtained with the Model Gas and Model Solid Fuel. (a) show a N-content (*x*-axis) from 0 to 1.4%; (b) is a zoom of the (a) graph for a N-content from 0 to 0.2%. The experimental data (red, orange, and green points) represent the three screenings performed at a lambda value of 1.15.

Model Solid Fuel demonstrates good agreement with the experimental data up to a total Fuel-N content of 0.1%, after which it underestimates the NO levels. On the other hand, Model Gas shows a strong correlation in the range of 0%−0.1% N-content, although it significantly underestimates NO levels above 0.1%. The Model Solid Fuel has a mixing profile much faster than that of the Model Gas. Consequently, Model Gas generates a larger oxygen-lean region than Model Solid Fuel, which subsequently restricts the formation of NO.

The underestimation of NO formation at low N-contents in Model Solid Fuel is explained by the low peak temperature of 1,400 °C, which gives almost no thermal NO formation, while Model Gas underestimates the level of NO for situations with Fuel-N content ≥0.1% (in mass). The rate of increase of NO along with the proportion of solid fuel in total fuel suggests that the flame characteristics in the experimental data may shift rapidly toward a more solid fuel flame profile following the addition of a small amount of solid fuel.

Furthermore, it is noteworthy that the introduction of solid fuel during the process of cofiring within an actual furnace can lead to significant alterations to the ignition point, the flame length and characteristics, the temperature profile, and the mixing profile. These ignition changes are discussed further in the next section.

Partitioning Fuel-NO and Thermal NO and the Nitrogen Pathway. Although commonly discussed as separate mechanisms, distinguishing between NO formation from the

fuel bound nitrogen and thermal NO formation from air borne N_2 is difficult as they share some reaction steps. Nevertheless, in this work, we attribute the difference in NO formation between the two cases, C_3H_8 and C_3H_8 + HCN, to the inclusion of HCN, representing Fuel-N.

For Model Gas with a Fuel-N content of 0.7%-mass, Fuel-N accounts for around 75% of the NO formation. When increasing the temperature (+100 °C), thermal formation increases, and the share of NO formation from Fuel-N decreases to 32%. In Model Solid Fuel, fuel-bound nitrogen is responsible for 99.6% of NO formation with the reference profile and 99.5% with the +100 °C profile. When the temperature of the Model Gas is decreased by 200 K (difference in temperature measured with the suction pyrometer at M2 between the lignite and propane flames, at a lambda value of 1.15), almost no NO is produced in the absence of added HCN.

Early Release of HCN. Figure 13 presents for both Model Gas (a) and Model Solid Fuel (b) the relationship between the outlet concentration of NO and the HCN release rate (1), the CO and O_2 concentrations along the reactions in the PFR (2), and the NO concentrations for the cases with HCN injections at 1, 30, 50, and 100 cm (3). Three combustion zones are defined to support the evaluation of the modeling results. Zone I is distinct from Zone II when the initial amount of oxidized O_2 is depleted by hydrocarbon oxidation. The separation of Zone II from Zone III starts when the highest NO concentrations are given by the respective HCN profiles with the reference temperature profile.

As a general observation, when HCN injection is completed in Zone I, the injection rate does not have any impact on the NO formation. If the injection is completed once the O_2 is depleted (in Zone II), NO formation is increased significantly, a minor reduction of NO attributed to the presence of CH radicals[21,24,63,65] within the high-temperature region (13−16 cm) is observed in the PFR. If the injection rate [HCN mixing profile >50 cm (gas) and >30 cm solid fuel] is even lower, such that it is completed in Zone III, the N-radicals released late in the PFR, are reacting with the NO, reducing the NO into N2 [eq 5]. Thus, in Zone III, injecting HCN at a later stage leads to more NO being reburned, resulting in a lower level of NO at the outlet. In the case of complete HCN injection at 200 cm, the NO concentration decreases to 1 ppm at the outlet.

These HCN injection profiles were tested with a higher temperature profile, with an increase of 100 K in the peak temperature (green) and with a higher Fuel-N content (increased from 0.7% to 1.4%). In Figure 14, both the increased temperature case and the increase Fuel-N case are compared with the reference cases. The *x*-axis represents the distances at which the HCN injections are completed in the PFR. A higher temperature in the PFR generates a higher level of NO and delays the peak of NO production by the corresponding HCN mixing profile from 50 to 60 cm for the Model Gas and 30 to 40 cm for the Model Solid Fuel. With a higher level of Fuel-N, the NO concentration in the outlet increases in Zone II and decreases in Zone III, thereby amplifying the formation and reduction of NO. However, it is interesting to note that when HCN is injected inside Zone I, no significant effect is seen on NO formation, which suggests that for a higher percentage of Fuel-N, the early release of fuel-volatile-N is even more important.

In both models, the formation of NO is highly dependent on the presence of OH when N-radicals are released. At around 10 cm in the PFR, eq 2 becomes active, increasing the levels of H
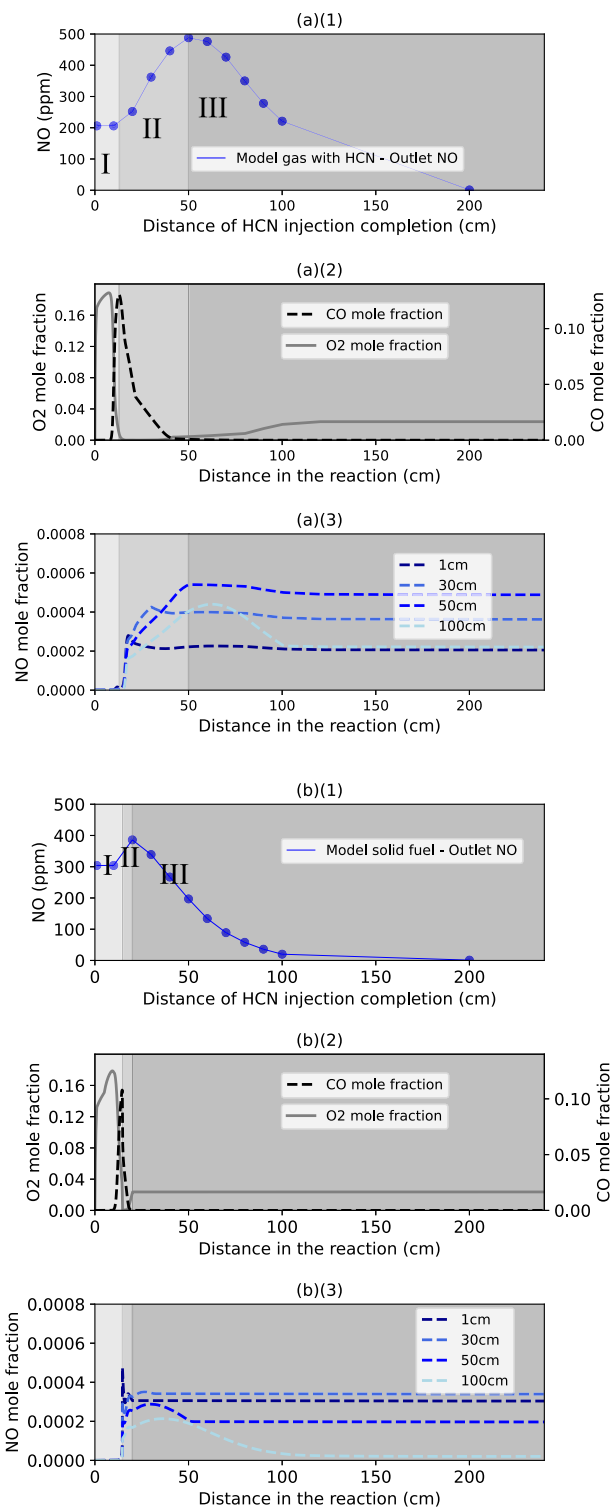
Figure 13. (a) Model Gas. (b) Model Solid Fuel. (**1**) NO concentrations in the outlet as a function of the distance at which HCN injection is completed in the plug flow reactor; (**2**) O_2 and CO concentrations as a function of the distance in the PFR; (**3**) NO concentrations as a function of the distances in the PFR for the cases in which HCN was injected at 1, 30, 50, and 100 cm.

radicals. These H radicals react with O_2 through eq 1 to form *OH + O*:

$$H + O_2 => OH + O \tag{1}$$
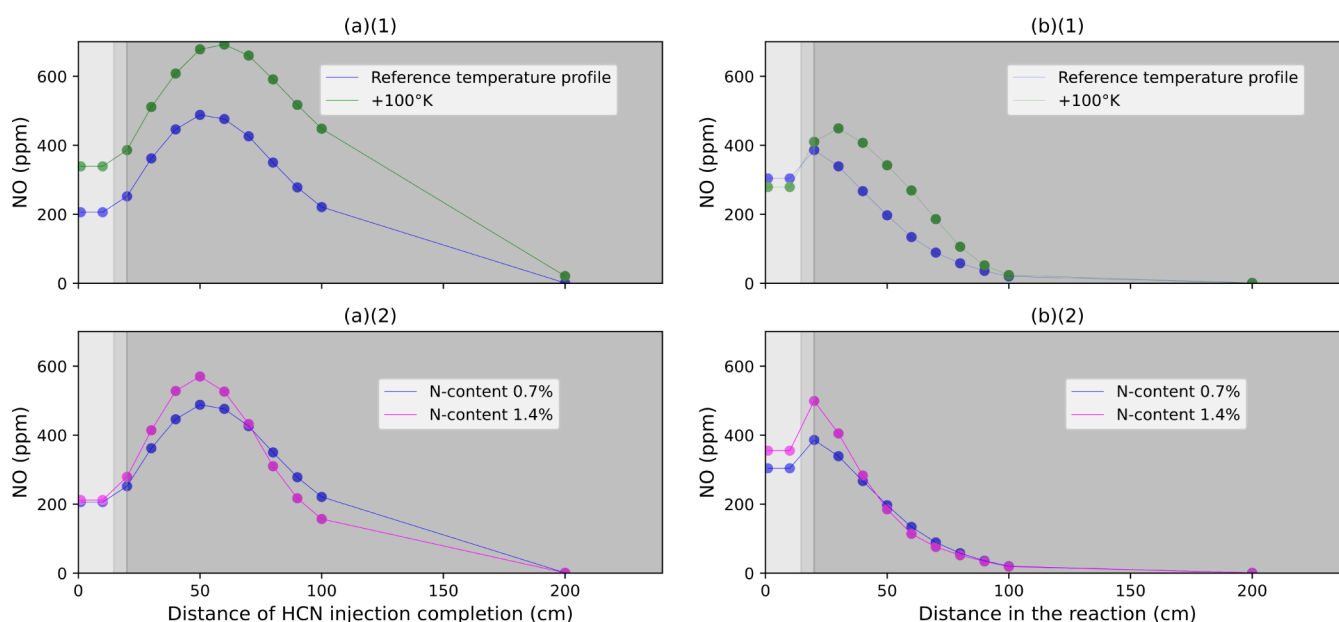
Figure 14. (a) Model Gas. (b) Model Solid Fuel. (**1**) Comparison of the NO concentrations in the outlet as a function of the HCN profiles with the reference temperature profile and a higher temperature profile (+100 K). (**2**) Comparison of the NO concentrations in the outlet as a function of the HCN profiles with Fuel-N concentrations of 0.7%-mass and 1.4%-mass.

$$CO + OH => CO_2 + H \qquad (2)$$

Furthermore, OH reacts with N, primarily derived from HCN, to form $NO + H$ [eq 3]. The presence of H radicals increases though both Eqs 2 and 3. When the HCN injection is completed in the zone with a high level of OH (Zone 2), the formation of NO is increased. In Zone III, the presence of OH decreases, resulting in the reaction of N from HCN with NO to form $N_2 + O$ or N, which leads to the reburning effect [eqs 4 and 5].

$$N + OH => NO + H \qquad (3)$$

$$N + NO => N_2 + N \qquad (4)$$

$$N + NO => N_2 + O \qquad (5)$$

A similar pattern is seen when increasing the peak temperature by 100 K, which suggests that the oxidizing/reducing conditions are the main driver of NO formation. However, the peak for NO is shifted slightly later under higher temperature conditions. This is attributed to a reduction mechanism that begins at a lower temperature, which occurs later with a higher temperature profile.

The results obtained from the models indicate that an early release of volatiles helps to limit the formation of NO. The reburning observed in Zone III is difficult to achieve in full scale due to the combination of an environment that has a high temperature and high level of O_2, which limits the possibility for late ignition of the solid fuel. Moreover, a very late injection of HCN leads to unwanted increases in the levels of NO_2 and N_2O in the flue gas.

■ DISCUSSION

The present study investigates the flame characteristics with particular attention on NO formation of replacing solid fuels with gaseous fuels in a 100 kW combustor. Specifically, it examines the relationship between thermal NO formation, which is promoted by gaseous fuels, and NO formation from fuel-bound nitrogen, which is promoted by solid fuels. In

addition, the study investigates the impacts of ignition and flame development on the conversion of volatile nitrogen species to NO.

While the oxidation of char-bound nitrogen is important for NO formation during pulverized coal combustion,[44,55] the conversion of char-bound nitrogen to NO or N_2 is believed to be less-affected by the combustion conditions, as compared to volatile nitrogen. Thus, the formation of NO from char-bound nitrogen is assumed to be mainly dependent upon the amount of introduced fuel-N.

The in-flame measurements clearly demonstrate that the ratio of gas to solid fuel significantly influences the flame shape. The addition of gas generally decreases the flame duration, which aligns with the expectations. Furthermore, at higher oxygen concentrations, the flame width is less-sensitive to the fuel ratio, and the flame width remains significant even during firing with pure propane.

The introduction of a gaseous fuel to a pulverized fuel flame increases the oxygen-lean zone and shifts it from the sides of the flame to the center of the flame. In the experimental unit, most of the volatile component derived from the solid fuel, in the form of HCN, was instead detected in the flame center when a gaseous fuel was introduced. Furthermore, the concentration of CO in the flame decreases as the proportion of the solid fuel increases.

As expected, the temperature of the lignite flame is significantly lower than that of the propane flame, yet the solid fuel flame produces a 6-fold higher level of NO. This shows that Fuel-N dominates NO formation through the thermal route, which is confirmed by the modeling. Similar conclusions have been drawn in a previous study of pulverized coal combustion, in which Fuel-N was deduced to be the major contributor to NO formation.[43] The addition of gaseous fuel to a solid fuel intrinsically decreases the Fuel-N and the resulting NO formation. However, since the studied gaseous fuels have higher adiabatic flame temperatures than bituminous coal, an increase in thermal-NO formation is expected. The models show a nonlinear relationship between NO formation and Fuel-N, with

a steep increase occurring when adding a small amount of HCN, which flattens at Fuel-N > 0.7%-mass when all the HCN is injected at the beginning of the PFR. Nonlinearity of the Fuel-N content with NO formation has also been reported by Kambara et al.[39] However, HCN released in an oxidative environment produces significantly greater amounts of NO.

The present study suggests that early ignition of solid fuels is beneficial in terms of reducing NO formation. Thus, the cocombustion of solid and gaseous fuels may be advantageous in that the gaseous fuels may facilitate faster ignition. However, it is important to note that the conditions in full-scale applications may differ with potentially higher temperatures and longer residence times at higher temperatures. The mixing profile may also be faster, which could have a negative impact on the NO formation, as shown by the models. In conclusion, when designing a low NO_x-combi-burner, it is crucial to consider an ignition process that occurs early and a mixing profile that progresses gradually. Azuhata and colleagues have also reported a gainful effect from the early ignition of NO_x emissions.[66]

CONCLUSION

This study characterizes flames during cocombusting a gaseous fuel with a solid fuel with a focus on the mechanisms of NO formation. The work combines detailed in-flame measurements of propane-lignite flames in a 100 kW unit and detailed reaction modeling to interpret and discuss the measurement results.

Overall, the results show that in cofiring conditions, it is favorable in terms of NO emissions to replace solid fuel with gaseous fuel, as this reduces the introduction of fuel-bound nitrogen to the flame. Moreover, if the combustion is designed so that the gaseous fuel is introduced to promote early ignition of the solid fuel while maintaining controlled mixing of the fuel and combustion air, NO formation may be reduced beyond the share of fuel-bound nitrogen avoided. In contrast, if the combustion process is designed such that the introduction of the gaseous fuel increases peak flame temperatures, then NO formation may be reduced to a lesser extent than the share of fuel-bound nitrogen avoided, as thermal NO formation is increased. This may even lead to an increase in the total NO formation. Therefore, controlling the NO emissions during the cofiring of solid and gaseous fuels is strongly dependent upon the burner design. Nevertheless, parameters such as the size distribution of the coal particles and the coal/air ratio in the coal flow may also play important roles.

Finally, the change in flame behavior obtained when supplementing a quantity of gas for a quantity of solid fuel appears to shift the flame to a "solid fuel" flame behavior by significantly decreasing the flame temperature and increasing the length of the flame. However, the in-flame concentration distribution of O_2, CO, and NO remains similar to a gas behavior, albeit more broadly spread.

AUTHOR INFORMATION

Corresponding Author

Samuel Colin − *Luossavaara-Kiirunavaara Aktiebolag, Luleå 97127, Sweden;* orcid.org/0009-0000-1371-8116; Email: samuel.colin@lkab.com, samuelco@chalmers.se

Authors

Fredrik Normann − *Division of Energy Technology, Department of Space Earth and Environment, Chalmers University of Technology, Göteborg SE-412 96, Sweden*

Christian Fredriksson − *Luossavaara-Kiirunavaara Aktiebolag, Luleå 97127, Sweden*

Klas Andersson − *Division of Energy Technology, Department of Space Earth and Environment, Chalmers University of Technology, Göteborg SE-412 96, Sweden;* orcid.org/ 0000-0001-5968-9082

Complete contact information is available at:
https://pubs.acs.org/10.1021/acsomega.4c01770

Notes

The authors declare no competing financial interest.

REFERENCES

(1) Schipper, E. L. F.; Revi, A.; Preston, B. L.; Carr, E. R.; Eriksen, S. H.; Fernández-Carril, L. R.; Glavovic, B.; Hilmi, N. J. M.; Ley, D.; Mukerji, R., et al. Climate Resilient Development Pathways. In *Climate Change 2022: Impacts, Adaptation and Vulnerability. Contribution of Working Group II to the Sixth Assessment Report of the Intergovernmental Panel on Climate Change*, Pörtner, H.-O.; Roberts, D. C.; Tignor, M. M. B.; Poloczanska, E. S.; Mintenbeck, K.; Alegría, A.; Craig, M.; Langsdorf, S.; Löschke, S.; Möller, V.; Okem, A.; Rama, B.; Cambridge University Press, 2022.

(2) Dias, V.; Pochet, M.; Contino, F.; Jeanmart, H. Energy and Economic Costs of Chemical Storage. *Front. Mech. Eng.* **2020**, *6*, 6.

(3) *Coal 2023 - Analysis and Forecast to 2026*; International Energy Agency, 2023.

(4) Levelized cost of energy by technology *Our World in Data*.https://ourworldindata.org/grapher/levelized-cost-of-energy. accessed 2024 April 23.

(5) Moraes, S. L. D.; Lima, J. R. B. D.; Ribeiro, T. R. Iron Ore Pelletizing Process: An Overview. In *Iron Ores and Iron Oxide Materials*, Shatokha, V. Ed.; InTech, 2018. DOI: .

(6) Canada, N. R. *Iron ore facts.* https://natural-resources.canada.ca/our-natural-resources/minerals-mining/minerals-metals-facts/iron-ore-facts/20517. accessed 2023 August 30.

(7) Ritchie, H.; Roser, M.; Rosado, P. CO_2 and Greenhouse Gas Emissions. *Our World In Data*, 2020. https://ourworldindata.org/co2-and-greenhouse-gas-emissions.

(8) Edland, R.; Smith, N.; Allgurén, T.; Fredriksson, C.; Normann, F.; Haycock, D.; Johnson, C.; Frandsen, J.; Fletcher, T. H.; Andersson, K. Evaluation of NOx-Reduction Measures for Iron-Ore Rotary Kilns. *Energy Fuels* **2020**, *34* (4), 4934−4948.

(9) de Vries, W. Impacts of Nitrogen Emissions on Ecosystems and Human Health: A Mini Review. *Curr. Opin. Environ. Sci. Health* **2021**, *21*, 100249.

(10) Wolfrum, J. Bildung von Stickstoffoxiden bei der Verbrennung. *Chem. Ing. Tech.* **1972**, *44* (10), 656−659.

(11) Konnov, A. A.; Colson, G.; De Ruyck, J. The New Route Forming NO via NNH. *Combust. Flame* **2000**, *121* (3), 548−550.

(12) Fenimore, C. P. Formation of Nitric Oxide in Premixed Hydrocarbon Flames. *Symp. (Int.) Combust.* **1971**, *13* (1), 373−380.

(13) *Gas-Phase Combustion Chemistry*, Gardiner, W. C.; Springer: New York, NY, 2000. DOI: .

(14) Pershing, D. W.; Wendt, J. O. L. Pulverized Coal Combustion: The Influence of Flame Temperature and Coal Composition on Thermal and Fuel NOx. *Symp. (Int.) Combust.* **1977**, *16* (1), 389−399.

(15) Merryman, E. L.; Levy, A. Nitrogen Oxide Formation in Flames: The Roles of NO2 and Fuel Nitrogen. *Symp. (Int.) Combust.* **1975**, *15* (1), 1073−1083.

(16) Rutar, T.; Lee, J. C. Y.; Dagaut, P.; Malte, P. C.; Byrne, A. A. NOx Formation Pathways in Lean-Premixed-Prevapourized Combustion of

Fuels with Carbon-to-Hydrogen Ratio between 0.25 and 0.88. *Proc. Inst. Mech. Eng., Part A* **2007**, *221* (3), 387−398.

(17) Westbrook, C. K.; Dryer, F. L. Simplified Reaction Mechanisms for the Oxidation of Hydrocarbon Fuels in Flames. *Combust. Sci. Technol.* **1981**, *27* (1−2), 31−43.

(18) Bowman, C. T. Control of Combustion-Generated Nitrogen Oxide Emissions: Technology Driven by Regulation. *Symp. (Int.) Combust.* **1992**, *24* (1), 859−878.

(19) Davidson, R. M. Nitrogen in Coal; IEA Coal Research, 1994.

(20) van der Lans, R. P.; Glarborg, P.; Dam-Johansen, K. Influence of Process Parameters on Nitrogen Oxide Formation in Pulverized Coal Burners. *Prog. Energy Combust. Sci.* **1997**, *23* (4), 349−377.

(21) Hill, S. C.; Douglas Smoot, L. Modeling of Nitrogen Oxides Formation and Destruction in Combustion Systems. *Prog. Energy Combust. Sci.* **2000**, *26* (4), 417−458.

(22) De Soete, G. G. Overall Reaction Rates of NO and N2 Formation from Fuel Nitrogen. *Symp. (Int.) Combust.* **1975**, *15* (1), 1093−1102.

(23) Edland, R.; Normann, F.; Fredriksson, C.; Andersson, K. Implications of Fuel Choice and Burner Settings for Combustion Efficiency and NOx Formation in PF-Fired Iron Ore Rotary Kilns. *Energy Fuels* **2017**, *31* (3), 3253−3261.

(24) Miller, J. A.; Bowman, C. T. Mechanism and Modeling of Nitrogen Chemistry in Combustion. *Prog. Energy Combust. Sci.* **1989**, *15* (4), 287−338.

(25) Howard, J. B.; Fong, W. S.; Peters, W. A. Kinetics of Devolatilization. In *Fundamentals of the Physical-Chemistry of Pulverized Coal Combustion*, Lahaye, J.; Prado, G.; Springer: Dordrecht, Netherlands, 1987; pp. 77103. DOI: .

(26) Jovanovski, G.; Boev, B.; Makreski, P. Chemistry and Geology of Coal: Nature, Composition, Coking, Gasification, Liquefaction, Production of Chemicals, Formation, Peatification, Coalification, Coal Types, and Ranks. *ChemTexts* **2023**, *9* (1), 2.

(27) Kambara, S.; Takarada, T.; Yamamoto, Y.; Kato, K. Relation between Functional Forms of Coal Nitrogen and Formation of Nitrogen Oxide (NOx) Precursors during Rapid Pyrolysis. *Energy Fuels* **1993**, *7* (6), 1013−1020.

(28) Zhang, H.; Fletcher, T. H. Nitrogen Transformations during Secondary Coal Pyrolysis. *Energy Fuels* **2001**, *15* (6), 1512−1521.

(29) Blair, D. W.; Wendt, J. O. L.; Bartok, W. Evolution of Nitrogen and Other Species during Controlled Pyrolysis of Coal. *Symp. (Int.) Combust.* **1977**, *16* (1), 475−489.

(30) Solomon, P. R.; Colket, M. B. Evolution of Fuel Nitrogen in Coal Devolatilization. *Fuel* **1978**, *57* (12), 749−755.

(31) Pohl, J. H.; Sarofim, A. F. Devolatilization and Oxidation of Coal Nitrogen. *Symp. (Int.) Combust.* **1977**, *16* (1), 491−501.

(32) Kimber, G. M.; Gray, M. D. Rapid Devolatilization of Small Coal Particles. *Combust. Flame* **1967**, *11* (4), 360−362.

(33) Pershing, D. W.; Wendt, J. O. L. Relative Contributions of Volatile Nitrogen and Char Nitrogen to NOx Emissions from Pulverized Coal Flames. *Ind. Eng. Chem. Proc. Des. Dev.* **1979**, *18* (1), 60−67.

(34) Spinti, J. P.; Pershing, D. W. The Fate of Char-N at Pulverized Coal Conditions. *Combust. Flame* **2003**, *135* (3), 299−313.

(35) Jensen, L. S.; Jannerup, H. E.; Glarborg, P.; Jensen, A.; Dam-Johansen, K. Experimental Investigation of NO from Pulverized Char Combustion: 28th International Symposium on Combustion. *Proc. Combust. Inst.* **2000**, *28* (2), 2271−2278.

(36) Brix, J.; Navascués, L. G.; Nielsen, J. B.; Bonnek, P. L.; Larsen, H. E.; Clausen, S.; Glarborg, P.; Jensen, A. D. Oxy-Fuel Combustion of Millimeter-Sized Coal Char: Particle Temperatures and NO Formation. *Fuel* **2013**, *106*, 72−78.

(37) Song, G.-L.; Lv, Q.-G.; Zhou, J.-H.; Cen, K.-F. Effect of Pulverized Coal Concentration on Emission Characteristics of NO x. In *Challenges of Power Engineering and Environment*, Cen, K.; Chi, Y.; Wang, F., Eds.; Springer: Heidelberg: Berlin, 2007; pp. 727732. DOI: .

(38) Adamczyk, W. P.; Werle, S.; Ryfa, A. Application of the Computational Method for Predicting NOx Reduction within Large Scale Coal-Fired Boiler. *Appl. Therm. Eng.* **2014**, *73* (1), 343−350.

(39) Kambara, S.; Takarada, T.; Toyoshima, M.; Kato, K. Relation between Functional Forms of Coal Nitrogen and NOx Emissions from Pulverized Coal Combustion. *Fuel* **1995**, *74* (9), 1247−1253.

(40) Tian, F.-J.; Yu, J.; McKenzie, L. J.; Hayashi, J.; Li, C.-Z. Formation of HCN and NH3 during the Reforming of Quinoline with Steam in a Fluidized-Bed Reactor. *Energy Fuels* **2006**, *20* (1), 159−163.

(41) Hampartsoumian, E.; Nimmo, W.; Clarke, A. G.; Williams, A. The Formation of NH3, HCN, and N2O in an Air-Staged Fuel Oil Flame. *Combust. Flame* **1991**, *85* (3), 499−504.

(42) Sun, L. S.; Shi, J.; Xiang, J.; Zhao, Q.; Hu, S.; Su, S. Study on the Release Characteristics of HCN and NH3 during Coal Gasification. *Asia-Pac. J. Chem. Eng.* **2010**, *5* (3), 403−407.

(43) Ledesma, E. B.; Li, C.-Z.; Nelson, P. F.; Mackie, J. C. Release of HCN, NH3, and HNCO from the Thermal Gas-Phase Cracking of Coal Pyrolysis Tars. *Energy Fuels* **1998**, *12* (3), 536−541.

(44) Hansson, K.-M.; Samuelsson, J.; Tullin, C.; Åmand, L.-E.; et al. Formation of HNCO, HCN, and NH3 from the Pyrolysis of Bark and Nitrogen-Containing Model Compounds. *Combust. Flame* **2004**, *137*, 265−277.

(45) McKenzie, L. J.; Tian, F.-J.; Li, C.-Z. Effects of Volatile−Char Interaction on the Formation of HCN and NH3 during the Gasification of Victorian Brown Coal in O2 at 500 °C. *Fuel* **2006**, *85* (14), 2148−2154.

(46) Nelson, P. F.; Li, C.-Z.; Ledesma, E. Formation of HNCO from the Rapid Pyrolysis of Coals. *Energy Fuels* **1996**, *10* (1), 264−265.

(47) Bassilakis, R.; Zhao, Y.; Solomon, P. R.; Serio, M. A. Sulfur and Nitrogen Evolution in the Argonne Coals. Experiment and Modeling. *Energy Fuels* **1993**, *7* (6), 710−720.

(48) Schäfer, S.; Bonn, B. Hydrolysis of HCN as an Important Step in Nitrogen Oxide Formation in Fluidised Combustion. Part 1. Homogeneous Reactions. *Fuel* **2000**, *79* (10), 1239−1246.

(49) Li, C.-Z.; Tan, L. L. Formation of NOx and SOx Precursors during the Pyrolysis of Coal and Biomass. Part III. Further Discussion on the Formation of HCN and NH3 during Pyrolysis. *Fuel* **2000**, *79* (15), 1899−1906.

(50) Thorne, L. R.; Branch, M. C.; Chandler, D. W.; Kee, R. J.; Miller, J. A. Hydrocarbon/Nitric Oxide Interactions in Low-Pressure Flames. *Symp. (Int.) Combust.* **1988**, *21* (1), 965−977.

(51) Miller, J. A.; Branch, M. C.; McLean, W. J.; Chandler, D. W.; Smooke, M. D.; Kee, R. J. The Conversion of HCN to NO and N2 in H2−O2−HCN−Ar Flames at Low Pressure. *Symp. (Int.) Combust.* **1985**, *20* (1), 673−684.

(52) Glarborg, P.; Jensen, A. D.; Johnsson, J. E. Fuel Nitrogen Conversion in Solid Fuel Fired Systems. *Prog. Energy Combust. Sci.* **2003**, *29* (2), 89−113.

(53) Li, C.-Z. Chapter 6 - Conversion of Coal-N and Coal-S during Pyrolysis, Gasification and Combustion. In *Advances in the Science of Victorian Brown Coal*, Li, C.-Z.; Elsevier Science: Amsterdam, 2004; pp. 286359. DOI: .

(54) Ueki, Y.; Yoshiie, R.; Naruse, I.; Matsuzaki, S. Effect of Hydrogen Gas Addition on Combustion Characteristics of Pulverized Coal. *Fuel Process. Technol.* **2017**, *161*, 289−294.

(55) Ren, M.; Liu, W.; Zhao, J.; Zou, C.; Ren, L.; Wu, H.; Zhao, J. Effects of Hydrogen Fraction in Co-Injection Gas on Combustion Characteristics of the Raceway in Low Carbon Emission Blast Furnace. *Int. J. Hydrogen Energy* **2023**, *48* (30), 11530−11540.

(56) Gan, M. J.; Liu, Y.; Shen, Y. A Novel Ironmaking Decarbonisation Technology — Co-Injection of Hydrogen and Biochar (CoHB): A CFD Study of Combustion in the Raceway under Simulated Blast Furnace Conditions. *Fuel* **2023**, *350*, 128745.

(57) Taniguchi, M.; Kozuma, T.; Takashima, Y.; Tsumura, T. Development of a Coal Combustion Model Compliant with the CHEMKIN Format for Use in Co-Firing Analysis with Hydrogen and Low-Carbon Fuels. *Energy Fuels* **2023**, *37* (1,), 657−666.

(58) Hesketh, R. P.; Davidson, J. F. The Effect of Volatiles on the Combustion of Char in a Fluidised Bed. *Chem. Eng. Sci.* **1991**, *46* (12), 3101−3113.

(59) Kremer, H.; Schulz, W. Influence of Temperature on the Formation of NOx during Pulverized Coal Combustion. *Symp. (Int.) Combust.* **1988**, *21* (1), 1217−1222.

(60) Nogami, H.; Yagi, J.; Kitamura, S.; Austin, P. R. Analysis on Material and Energy Balances of Ironmaking Systems on Blast Furnace Operations with Metallic Charging, Top Gas Recycling and Natural Gas Injection. *ISIJ Int.* **2006**, *46* (12), 1759−1766.

(61) de Castro, J. A.; Nogami, H.; Yagi, J. Numerical Investigation of Simultaneous Injection of Pulverized Coal and Natural Gas with Oxygen Enrichment to the Blast Furnace. *ISIJ Int.* **2002**, *42* (11), 1203−1211.

(62) Edland, R.; Normann, F.; Andersson, K. Modeling the Contributions of Volatile and Char-Bound Nitrogen to the Formation of NOx Species in Iron Ore Rotary Kilns. *Energy Fuels* **2018**, *32* (2), 2321−2331.

(63) Normann, F.; Andersson, K.; Johnsson, F.; Leckner, B. Reburning in Oxy-Fuel Combustion: A Parametric Study of the Combustion Chemistry. *Ind. Eng. Chem. Res.* **2010**, *49* (19), 9088− 9094.

(64) Mendiara, T.; Glarborg, P. Ammonia Chemistry in Oxy-Fuel Combustion of Methane. *Combust. Flame* **2009**, *156* (10), 1937−1949.

(65) Glarborg, P.; Miller, J. A.; Ruscic, B.; Klippenstein, S. J. Modeling Nitrogen Chemistry in Combustion. *Prog. Energy Combust. Sci.* **2018**, *67*, 31−68.

(66) Azuhata, S.; Narato, K.; Kobayashi, H.; Arashi, N.; Morita, S.; Masai, T. A Study of Gas Composition Profiles for Low NOx Pulverized Coal Combustion and Burner Scale-Up. *Symp. (Int.) Combust.* **1988**, *21* (1), 1199−1206.